Effects of free carriers on the optical properties of high mobility transition metal doped In_2O_3 transparent conductors

Kingsley O. Egbo,[1] Ayotunde E. Adesina,[2] Chioma V. Ezeh,[1] Chao Ping Liu,[3] and Kin Man Yu[1,2,*]

[1]*Department of Physics, City University of Hong Kong, 83 Tat Chee Avenue, Kowloon, Hong Kong*

[2]*Department of Material Science and Engineering, City University of Hong Kong, Kowloon, Hong Kong*

[3]*Research Center for Advanced Optics and Photoelectronics, Department of Physics, College of Science, Shantou University, Shantou, Guangdong 515063, China*

(Received 23 April 2021; accepted 25 August 2021; published 17 September 2021)

Transition metal doped In_2O_3 with high mobility can be used as a transparent conductor with enhanced transparency spectral window. In this work, we carried out a comprehensive study on the electrical and optical properties of In_2O_3 doped with several transition metal (TM) species (In_2O_3 : TM) including W, Zr, Mo, and Ti. Detailed optical properties obtained by spectroscopic ellipsometry (SE) are correlated with electrical properties obtained by Hall effect measurements. We find that the mobility of In_2O_3 : TM thin films lies in the range of 50–75 $cm^2\,V^{-1}\,s^{-1}$, much higher than the typical mobility of 30–40 $cm^2\,V^{-1}\,s^{-1}$ for conventional ITO. The complex dielectric functions of the thin films reveal remarkable carrier density dependent changes in the optical properties. SE analyses show that the electron effective mass of In_2O_3 : TM at the bottom of the conduction band m_o^* (0.11–0.14m_o) is much smaller than the reported $m_o^* \sim 0.18-0.30m_o$ for ITO, which directly results in their higher mobility. This low m_o^* is consistent with recent theoretical studies which proposed that 4*d* donor states of the TMs are resonance in the CB. For films with comparably low resistivity of 1–2 $\times\ 10^{-4}\ \Omega$ cm, we find that In_2O_3 : TM films have ∼4–10 times lower absorption coefficient at $\lambda = 1300$ nm due to free carrier absorption and have their plasma reflection edge extended to ∼1.7 μm compared to ∼1.2–1.4 μm for ITO. Hence, using TM doping we have achieved transparent conductors with conductivity comparable to ITO but with transmission extended to >1600 nm. These materials will be potentially important as transparent conductors for optoelectronic devices utilizing NIR photons.

DOI: 10.1103/PhysRevMaterials.5.094603

I. INTRODUCTION

Transparent conductive oxides (TCOs) which show high conductivity and visible light transparency have been applied as essential components and electrodes in many optoelectronic devices such as touch screen displays, low-emissivity windows and solar cells [1,2]. In_2O_3-based transparent conductors show great potentials for applications and In_2O_3 : Sn (ITO) with its high transparency, high carrier concentration and low resistivity is the dominant transparent conducting oxide in the market. ITO can be deposited on large area amorphous and polymer substrates and it can achieve a low resistivity of $\sim 10^{-4}\ \Omega$ cm with visible light transmittance greater than ∼80%, these desirable properties make ITO an excellent transparent conductor material [3–5]. Moreover, ITO also has a high work function which supports its application as transparent electrodes in many energy device systems [6]. However, polycrystalline ITO thin films with high conductivity ($\sim 1 \times 10^4$ S/cm) have moderate to low mobility ($< 40\ cm^2\,V^{-1}\,s^{-1}$) and poor transmittance in the NIR spectrum ($\lambda > 1100$ nm) [7]. It has been suggested that the low mobility in ITO arises from the strong hybridization of the Sn-5*s* and In-5*s* orbitals which leads to a larger effective mass due to a broadening of the conduction band dispersion [8]. Since the conductivity depends on the product of carrier concentration and mobility, in order to achieve high conductivity for a material with low mobility, a high electron concentration is needed. The high density of Sn dopants (∼10%) required to achieve very high carrier concentration ($>10^{21}\ cm^{-3}$) results in strong ionized impurity scattering, which further reduces the carrier mobility. As a consequence of the high carrier concentration, plasma reflection and free carrier absorption effects in this material limit its long wavelength applications. Hence, to maximize optical transparency across a large spectral range, materials with high mobility is desirable as this would lead to high conductivity with lower carrier concentration than ITO.

Transition metal (TM) (e.g., Ti, W, Mo) doping in In_2O_3 (In_2O_3 : TM) has been shown to lead to improved mobility compared to ITO. A number of studies on the electrical and optoelectronic properties of transition metal (TM) doped In_2O_3 thin films have been reported [9–20]. In general, these transition metal doped In_2O_3 thin films have lower carrier concentration of typically $\lesssim 5 \times 10^{20}\ cm^{-3}$ but improved mobility (as high as $\sim 80\ cm^2\,V^{-1}\,s^{-1}$), resulting in comparable conductivity with high quality ITO [8]. As a consequence, the optical transparency of In_2O_3 : TM covers a wider spectral window, extending to the IR region (∼1500 nm). However, detailed studies of the effects of different TM dopant on the optoelectronic properties of In_2O_3

*kinmanyu@cityu.edu.hk

are still lacking. Furthermore, free carriers in TCOs with high carrier concentration ($\sim 10^{20}$–10^{21} cm^{-3}) are also known to play remarkable roles in their optical properties [21,22]. For instance, such effects as free carrier absorption at low energies and a blue shift of the band edge influence the determinations of their optical properties. But a comprehensive look at the effect of free carriers on the optical properties of these high mobility TM doped In_2O_3 is yet to be reported.

In this study, we explore the effects of different TM dopants including W, Mo, Zr, and Ti on the transport and optoelectronic properties of sputter deposited polycrystalline In_2O_3 thin films. The electrical characterization was carried out by Hall effect measurements and the detailed optical analysis was carried out by standard Spectroscopic ellipsometry (SE) measurements. SE offers a reliable technique for the accurate determination of optical properties of thin films and bulk samples. It has been used to extensively study the optical properties of metal oxide materials as well as the effects of free carriers on highly doped transparent conducting metal oxides [21–24]. In SE, by fitting the measured amplitude and phase difference of the ratio of the polarization state of the reflected and incident light over a wide spectral range using appropriate models, the real and imaginary parts of the complex dielectric function of the film can be obtained. From the dielectric function, various material properties such as the high-frequency dielectric constant, absorption coefficient, the optical gap, the optical mobility, the electron effective mass, and plasma reflection edge can be extracted.

Our Hall measurements show that electron concentration in the range of 1.2–8.2×10^{20} cm^{-3} and mobility of up to 75 cm^2/V-s were achieved in these In_2O_3 : TM thin films. Compared to ITO thin films, these In_2O_3 : TM have comparable conductivity but much lower carrier concentration and higher mobility, and hence their transmittance can be extended to >1500 nm in the IR region with no observable free carrier absorption and plasma reflection. The higher mobility of In_2O_3 : TM can be primarily attributed to their lower effective mass and the differences in the mobility for various In_2O_3 : TM thin films are explained in terms of the nature of the interaction of the TM dopants with the host conduction band. Detailed effects of free carriers in these high mobility In_2O_3 : TM were explored by SE, and these results offer further insights into the optical properties of these thin films.

II. EXPERIMENT

Transition metal doped In_2O_3 thin films were deposited by magnetron co-sputtering using a dual-gun radio-frequency magnetron sputtering system. All samples were grown at a substrate temperature of ~220 °C on precleaned glass substrates. W, Mo, Zr, and Ti doping was achieved by using metal targets of these elements sputtered in the DC mode during the RF sputtering of an In_2O_3 ceramic target. Since the electron density of doped In_2O_3 is also affected by native defects, our sputtered thin film samples were annealed in N_2 gas using a rapid thermal annealing (RTA) system. Optimum electrical properties were obtained for thin films RTA at 650 °C for 90 s, and all further characterizations presented in this study were performed on these "optimized samples." Also note that, the maximum annealing temperature used in this study is limited by the glass substrates which would undergo glassy transition at ~750 °C in RTA.

Dopant concentrations were determined by x-ray fluorescence (XRF) and x-ray photoelectron spectroscopy (XPS) measurements [25]. Film thicknesses in the range of 70–180 nm were estimated from an optical profilometry and confirmed by SE modeling. Grazing Incidence x-ray diffraction (GIXRD) with an incident angle of 1 ° was used to obtain the x-ray diffraction spectra of the thin films as shown in Fig. S1 of Ref. [26]. The diffraction spectra showed that all the films are polycrystalline with the cubic bixbyite In_2O_3 structure with typical grain size in the range of 16–20 nm as calculated using the Scherrer equation. To characterize the electrical properties of our thin films, Hall effect measurements in the *van der Pauw* configuration were carried out using a Ecopia HMS5000 Hall system with a magnetic field, $B = 0.54$ T. The optical properties were characterized by room temperature standard Spectroscopic ellipsometry in the spectra range of 0.73 to 6.5 eV using a J.A.Woollam RC2 system. The angle of incidence was varied from 55 ° to 75 ° with an increment of 10 °. Translucent plastic tapes were used to eliminate backside reflection on the glass substrates.

III. SE ANALYSIS

Due to the high carrier concentration $\sim 10^{20}$–10^{21} cm^{-3} in heavily doped TCOs, the Drude model which describes the optical response of free electrons in metal-like materials has been successfully used to describe TCO materials in combination with other models describing contributions from inter-band optical transitions [21,22]. Equation (1) is the expression of the complex dielectric function in the Drude free electron model used to describe the optical properties in TCOs with high carrier concentration which has the form of a Lorentz oscillator with zero center energy [27];

$$\varepsilon(E) = \varepsilon_1(E) - i\varepsilon_2(E) = \varepsilon_\infty - \frac{A_D}{E^2 - i\Gamma_D E} \tag{1}$$

In Eq. (1), the amplitude, A_D and the broadening, Γ_D are the two free parameters, while the term ε_∞ is the high-frequency dielectric constant. Based on the Drude theory, A_D can be expressed as $A_D = \varepsilon_\infty {E_p}^2$, where E_p is the plasma energy which corresponds to the energy at which the real part of the dielectric function drops from positive to negative values. This characteristic Drude metal-like optical property depends on the carrier concentration and occurs in the near infrared (NIR) to mid-IR frequencies in TCOs. The frequency at which this transition occurs is called the epsilon-near-zero (ENZ) frequency, which corresponds to the plasma frequency, ω_p. The plasma energy E_p can be related to the optical carrier concentration N_{opt}, and the electron effective mass m^* as

$$E_p = \hbar\omega_p = \sqrt{\frac{\hbar^2 e^2 N_{\text{opt}}}{m^* \varepsilon_0 \varepsilon_\infty}}, \tag{2}$$

where $\hbar$, e, and ε_0 are the reduced Plank's constant, electron charge and vacuum permittivity, respectively. The dielectric function according to the Drude model in Eq. (1) can also be

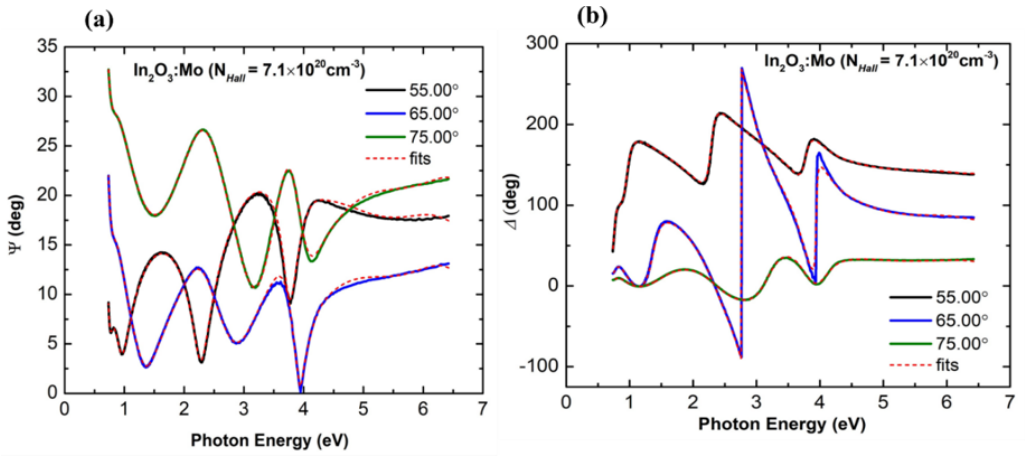

FIG. 1. The measured and fitted (red dashed lines) SE spectra [Ψ and Δ in (a) and (b), respectively] of In_2O_3:Mo thin film with $N_{Hall} = 7.1 \times 10^{20}$ cm^{-3} for angle of incidence: 55 °, 65 °, and 75 °.

described in terms of the optical resistivity ρ_{opt} and the mean scattering time, τ as [28]

$$\varepsilon(E) = \varepsilon_1(E) - i\varepsilon_2(E) = \varepsilon_\infty - \frac{\hbar^2}{\varepsilon_0 \rho_{opt}(\tau E^2 - i\hbar E)}, \quad (3)$$

where the optical carrier concentration, optical carrier mobility and electron effective mass are related to the optical resistivity as follows:

$$\rho_{opt} = \frac{m^*}{N_{opt}\, e^2 \tau} = \frac{1}{e N_{opt}\, \mu_{opt}}. \quad (4)$$

The complex dielectric functions of the In_2O_3 : TM thin films were obtained by fitting the SE spectra (i.e., the amplitude ratio Ψ and the phase difference Δ). A three-layer structure comprising a thin surface roughness layer, the bulk In_2O_3 film layer and the glass substrate was used for the data analysis using the *CompleteEASE* software. The line shape of the layer dielectric functions, and the thickness of the thin film layer were first estimated using a numerical B-spline approximation. The layer thickness was kept fixed and the dielectric function parameters were used as adjustable parameters for the fittings. SE data obtained from different incident angles were fitted simultaneously. An oscillator model composed of a combination of a Drude model and two Tauc-Lorentz models were then used to parameterize the dielectric function. Figure 1 shows typical experimental SE spectra (solid lines) taken at different incident angles and dielectric function oscillators fitting (dashed red lines) of a In_2O_3:Mo thin film with carrier density $\sim 7 \times 10^{20}$ cm^{-3}. From Fig. 1, it is evident that the adopted dielectric function oscillator parameters shown in Table S1 of Ref. [26] can fit the experimental SE data well across the measured spectral range.

IV. RESULTS AND DISCUSSION

A. Electrical properties of TM doped In_2O_3

The electrical properties of magnetron sputtered polycrystalline W, Mo, Zr, and Ti doped In_2O_3 thin films after RTA in N_2 at 650 °C for 90 s are shown in Fig. 2. The electrical properties of these In_2O_3 : TM thin films improve with annealing compared to the as-grown samples likely because of improved crystallinity and substitution of the dopants in the

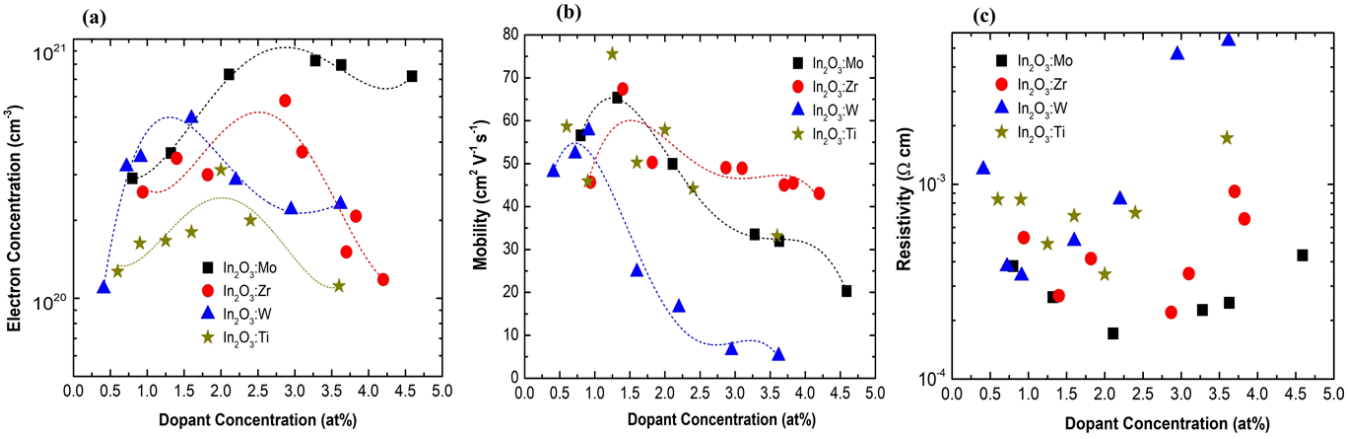

FIG. 2. Electron concentration N_H (a) mobility μ_H (b) and resistivity ρ (c) for In_2O_3 thin films doped with TM dopants (Ti, W, Mo, and Zr) with increasing dopant concentration N_d. Dashed lines are guide to the eyes.

TABLE I. A comparison of values of several experimentally obtained electrical properties, plasma energy, E_p and electron effective mass, m* of TM doped In_2O_3 reported in the literature using different deposition techniques.

Dopant	Conc.	Dep.[a] Technique	T_g(°C)	N(cm^{-3})	μ(cm^2 V^{-1} s^{-1})	ρ(Ω-cm)	E_p(eV)	m*	Ref.
Mo	1 mol%	AACVD	450	3.1×10^{20}	107	1.9×10^{-4}	–	–	[17]
Mo	5wt%	Thermal Evaporation	350	4×10^{20}	>100	2.1×10^{-4}	0.56	–	[34]
Mo	0.7 at%	[b]Mist-CVD	400	2.2×10^{20}	89	3.2×10^{-4}	–	–	[35]
Mo	1.3 at%	RF Sputtering	500	1.5×10^{20}	93	4.4×10^{-4}	0.33	–	[35]
Mo	0.5 at%	[b]Spray Pyrolysis	400	9.5×10^{19}	122.4	5.3×10^{-4}	–	–	[9]
Mo	2 wt%	RF Sputtering	450	3.0×10^{20}	83	–	–	0.32	[36]
Mo	0.5 at%	[b]Spray Pyrolysis	400	1.0×10^{20}	149	4.0×10^{-4}	–	–	[37]
Mo	2 wt%	RF Sputtering	RT	5.2×10^{20}	20	–	–	–	[38]
Mo	1.3mol%	[b]RF Sputtering	220	3.6×10^{20}	65	2.6×10^{-4}	0.65	0.3	Thiswork
Zr	0.2at %	PLD	650	$\sim 3.0 \times 10^{20}$	~70	$\sim 3.0 \times 10^{-4}$	–	–	[15]
Zr	1-2 wt%	RF sputtering	~600	$\sim 5.0 \times 10^{20}$	~75	$\sim 1.6 \times 10^{-4}$	–	–	[39]
Zr	1.4 mol at%	[b]RF Sputtering	220	3.4×10^{20}	67	2.7×10^{-4}	0.52	0.25	This work
Ti	1.7 at%	RF Sputtering	550	1.5×10^{20}	83.3	2.6×10^{-4}	~0.56	–	[40]
Ti	1wt%	[b]RF Sputtering	500	3.06×10^{20}	105	1.95×10^{-4}	–	–	[13]
Ti	1.2mol%	[b]RF Sputtering	220	1.7×10^{20}	75	4.9×10^{-4}	0.5	0.2	This work
W	~3.5wt%	DC Sputtering	320	2.8×10^{20}	67	3.1×10^{-4}	–	–	[41]
W	0.5 at%	[b]Spin Coating	RT	5.0×10^{20}	23	5.3×10^{-4}	–	–	[42]
W	0.03	PLD	400	2.9×10^{20}	66	3.2×10^{-4}	–	0.3	[43]
W	1.15wt%	RPD	200	$\sim 1.4 \times 10^{20}$	80	–	~0.41	–	[14]
W	0.91mol %	[b]RF Sputtering	220	3.5×10^{20}	58	3.3×10^{-4}	0.64	0.28	This work

[a]AACVD = Aerosol-assisted chemical vapor deposition, T_g = Growth temperature. PLD = Pulsed Laser deposition, RPD = Reactive plasma deposition.
[b]Post deposition annealed.

cation site. It is also likely that annealing in N_2 led to the formation of O vacancies which are known to be donorlike defects in Indium oxide and other metal oxides and these native defects can play significant roles in controlling their electrical properties [29,30]. Similar electrical properties improvement by post-deposition annealing have been reported for other oxide transparent conductors [31]. However, we also note that in most cases native defects formed and H donors incorporated due to annealing are on the order of $<10^{20}$ cm^{-3} [32], which is lower than the electron concentration we observed in these In_2O_3 : TM films. Figure S2 (see Ref. [26]) shows changes in the electrical properties of In_2O_3 : TM thin films with annealing temperature up to 650 °C.

The electrical properties obtained by room temperature Hall measurements are plotted as a function of doping concentration N_d given in cation mole % ([TM]/[In+TM] %) for the various TM dopants in Fig. 2. As shown in Fig. 2(a), the magnitude of the Hall measured carrier concentration N_H varies with different TM dopants, but in general the change in the carrier concentration with doping concentration N_d shares a similar trend, showing an increase of N_H with N_d up to a peak N_H value and a subsequent drop as N_d further increases. W doped In_2O_3 shows a maximum N_H of 4.5×10^{20} cm^{-3} at a $N_d \sim 1.5\%$ with a subsequent decrease at higher N_d, while a maximum N_H values of 5.8×10^{20} and 8.2×10^{20} cm^{-3} are obtained for ~3% Zr and Mo doping, respectively.

High Hall mobility values $\mu_H = 75$ and 68 cm^2 V^{-1} s^{-1} are achieved for Ti and Zr doping, respectively at a N_d of ~1.5% as shown in Fig. 2(b). Mo doped sample also shows a high mobility at a similar N_d range with a maximum value of ~65 cm^2 V^{-1} s^{-1}, while a maximum μ_H of 58 cm^2 V^{-1} s^{-1} is obtained for W doping at a N_d of ~1%. The differences in the carrier mobility at similar N_d (1%–1.5%) for different TM dopants can be understood in terms of the nature and interaction of the TM d states with In 5s due to the location of the d-states of the different TM dopants above the conduction band minimum (CBM). From the theoretical work of Xu *et al.,* and Swallow *et al.,* they identified that d-state levels of Mo, are located at resonant positions high above the CBM. This leads to negligible interaction of these d states with the 5s states so that the CB dispersion is not disturbed, and this gives rise to a smaller effective mass which in turn leads to higher mobility values [8,33]. Xu *et. al.*, further showed that unlike in Zr and Mo, d-states of W-dopant lie closer to the CBM of the host material, and hence a non-negligible hybridization is expected which may broaden the CB dispersion and lowers the mobility in In_2O_3:W. We note that reported RT mobility for polycrystalline ITO lies between 20–40 cm^2 V^{-1} s^{-1} [4,12,14], and the maximum RT μ_H obtained for our In_2O_3 : TM films have significantly higher μ_H values. Table I compares highest mobility values for our TM doped In_2O_3 with previously reported works in the literature. In general high mobility have been reported for these TM doped In_2O_3 polycrystalline thin films and the reported mobilities increases with growth temperatures for similar dopant concentration

From Fig. 2(b), the μ_H of all In_2O_3 : TM films also shows a remarkable decrease with increasing N_d. This mobility drop has also been observed in other TM doped metal oxides [44–47]. Li *et al.,* compared In and V doping in CdO and found that while the mobility in In doped CdO increased slightly with doping from ~100 to 120 cm^2 V^{-1} s^{-1} and stabilized at ~80 cm^2 V^{-1} s^{-1} as the dopant concentration increased, the mobility of V doped CdO dropped rapidly from 100 to ~10 cm^2 V^{-1} s^{-1} at ~10% V doping [44]. This difference in

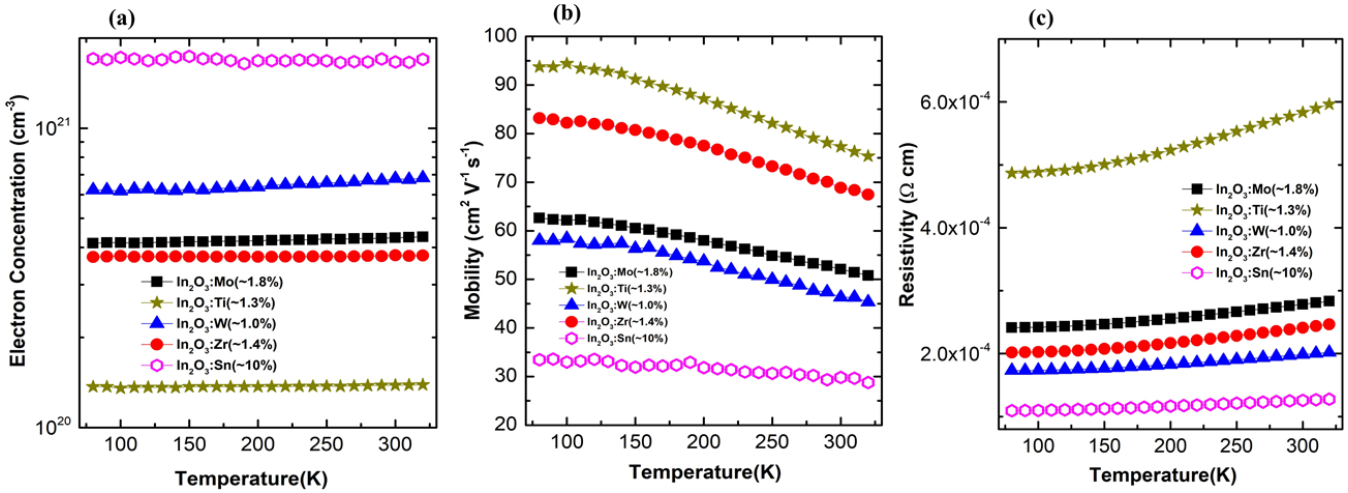

FIG. 3. Temperature dependence of (a) Electron concentration (b) Mobility and (c) resistivity of ∼1%–2% TM doped In_2O_3 thin films with high mobilities. Data for ITO is shown in open symbol for comparison.

the behavior of the mobility with increasing dopant concentrations was attributed to the modification of the CdO conduction band (CB) due to the anticrossing interaction between the V localized d states and the CdO extended conduction band states. This anticrossing interaction results in the restructuring of CdO CB, leading to a drastic decrease in the mobility due to the large effective mass of the modified CdO. Similar anticrossing interaction between TM d states with oxide CB was also reported for V doped ZnO [45]. Such anticrossing interaction may also be responsible for the large drop in the mobility in our In_2O_3 : TM at high doping concentration (>2.5%) as shown in Fig. 2(b).

Figure S3 [26] shows a plot of the mobility as a function of electron concentration obtained by Hall effect measurements for our In_2O_3 : TM and ITO thin films. From the plot, a general trend of decreasing mobility with increasing electron concentration is observed and this is likely due to the increased ionized impurities scattering. However, at low carrier concentration, some In_2O_3 : TM thin films such as In_2O_3:W and In_2O_3:Zr show a large spread in the data with some increase in mobility indicating that grain boundary scattering and other additional scattering is not negligible at these low dopant concentration [48,49].

Figure 3 shows the variable temperature Hall data obtained for In_2O_3 : TM films with $N_d \sim 1.0\%$–2.0% at which the highest μ_H was obtained. As expected, due to the degenerate nature of the In_2O_3 : TM films, no observable temperature dependence on the N_H is evident as shown in Fig. 3(a). In contrast, Fig. 3(b) shows a decrease in μ_H with increasing temperature for all In_2O_3 thin films. This decrease in mobility is more evident in the In_2O_3:Ti thin film with higher μ_H and is least observable in the lower μ_H ITO. The large decrease in μ_H for In_2O_3:Ti can be attributed largely to phonon scattering. At the temperature range studied, $\geqslant 80$ K, ionized impurity scattering is negligible, however the plateau observed between 80–100 K indicates that at lower temperatures <80 K, μ_H may be limited by ionized impurity scatterings. Consequently, a slight increase in resistivity with temperature is seen in Fig. 3(c) due to μ_H dominated by phonon scattering.

B. Complex dielectric function, plasma energy, and high-frequency dielectric function

The real and imaginary parts of the complex dielectric function of In_2O_3:Mo thin films with different N_H are shown in Figs. 4(a) and 4(b), respectively. The peak of the ε_1 spectra at ∼4 eV shifts slightly to higher energy with increasing N_H, indicating an increase in the optical gap. The plasma energy, E_p can be extracted at the photon energy where $\varepsilon_1(E) = 0$ as shown in the inset of Fig. 4(a). Due to SE equipment limitation in the IR range, the plasma energy could not be extracted directly using the measured spectra for films with $N_H < 4.8 \times 10^{20}$ cm^{-3}. For these In_2O_3 : TM films with low N_H, in order to extract their plasma energy, $\varepsilon_1(E)$ were extrapolated to zero by simulating the experimental $\varepsilon_1(E)$ data across the desired spectra range using the CompleteEASE software as shown by the dashed red lines in the inset of Fig. 4(a). Figure 4(b) shows the imaginary part of the dielectric function $\varepsilon_2(E)$. An increase in $\varepsilon_2(E)$ at low IR energy with increasing N_H is observed signifying a non-negligible free carrier absorption which will be discussed later.

The inset of Fig. 4(a) shows that the plasma energy of the In_2O_3:Mo films increases with increasing N_H up to 8.2×10^{20} cm^{-3} for increasing Mo dopant concentration in In_2O_3. At higher N_d the N_H drops slightly back to 7.0×10^{20} cm^{-3}, leading to a slight decrease in the E_p. The plasma wavelength λ_p obtained for different In_2O_3 : TM thin films with accuracies, $\pm 0.25\,\mu$m are plotted as a function of film resistivity ρ in Fig. 5(a). Previously reported values of λ_p for other transparent conducting metal oxide materials (In_2O_3 : Sn, and CdO:In) are also shown for comparison. A general trend of a monotonous decrease of the λ_p with decreasing ρ is observed for all the TCO samples. From Eq. (2), λ_p can also be related to ρ and the mobility μ as follows:

$$\lambda_p = 2\pi c\sqrt{\frac{m^*\varepsilon_\infty\varepsilon_o}{e^2 N_{\text{opt}}}} = 2\pi c\sqrt{\frac{m^*\varepsilon_\infty\varepsilon_o\mu\rho}{e}}, \qquad (5)$$

where c is the speed of light. Figure 5(a) shows that the plasma edge decreases to lower wavelength when the resistivity decreases as expected, due to the increase in carrier

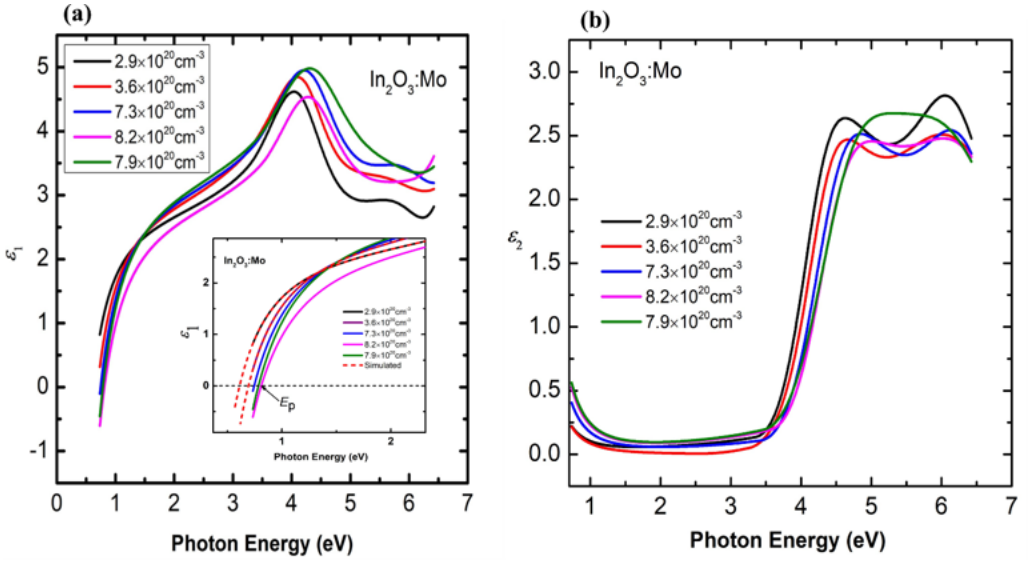

FIG. 4. Complex dielectric function of In_2O_3:Mo thin films showing (a) the real dielectric function and (b) imaginary part of the dielectric function with the variable N_{Hall}. The inset of Fig. 3(a) shows the extrapolation of the plasma energy of the thin films.

concentration. Since the In_2O_3 : TM films have higher mobility than In_2O_3 : Sn and CdO:In, they also show a higher λ_p for a given ρ. For example, for a low $\rho \sim 1$–$4 \times 10^{-4}\,\Omega\,\text{cm}$, λ_p is in the range of 1.2–1.6 μm for ITO but extends to $\sim$1.7 to 2 μm for In_2O_3 : TM films. Hence, because of their higher mobility, In_2O_3 : TM films can achieve a much wider transparency window into the near infrared spectral range compared to ITO with comparable electrical conductivity.

At sufficiently low photon energies, according to the Drude model, the real part of the dielectric function can be expressed as $\varepsilon_1(E) = \varepsilon_\infty - A_D/(E^2 + \Gamma_D^2)$, where A_D is the Drude amplitude and Γ_D is the broadening. This allows us to obtain the high-frequency dielectric constant ε_∞ from the intercept of the ε_1 versus $1/E^2 + \Gamma_D^2$ plot [21]. The values of ε_∞ obtained from the intercepts of such plots for different In_2O_3 : TM thin films are shown in Fig. 5(b). At low frequencies, the dielectric function of a material has significant contributions from electrons, ions and dipoles, etc. However, at high frequencies, only electrons can respond, and hence the dielectric constant at high-frequency depends strongly on the electron concentration. Although the incorporation of small number of dopants does not significantly change the overall composition and structure of the material, it increases the electron concentration significantly [50]. Values of ε_∞ for In_2O_3 doped with different species (TM and Sn) fall within the range of $\sim$4.8–3.8 and follow a general trend of lower ε_∞ as N_H increases. However, slight differences in ε_∞ are observed for different TM dopants with similar carrier density. Similar dependence of the high-frequency dielectric constant on carrier density have been reported earlier for transparent conducting metal oxides [21]. The obtained high-frequency dielectric constant of our ITO of $\sim$3.85 shown are in

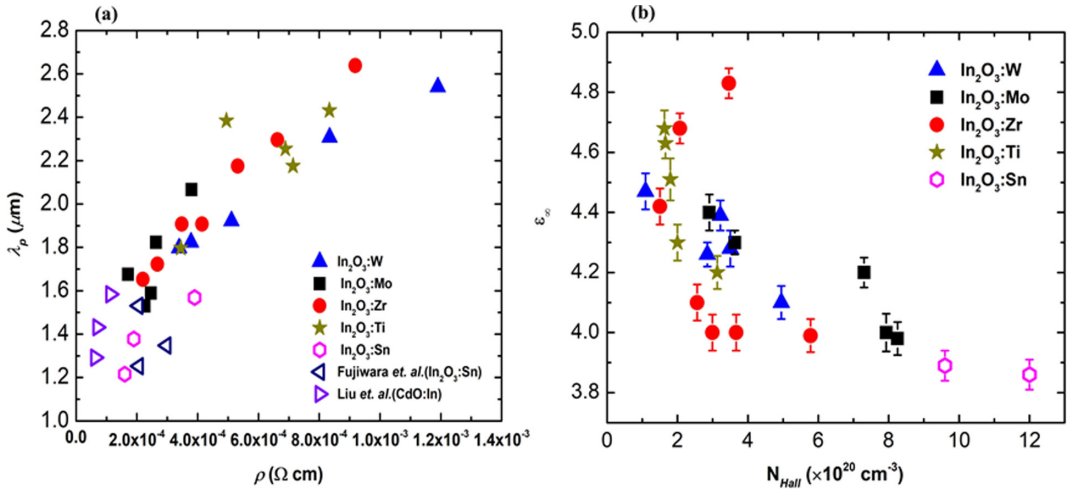

FIG. 5. (a): The plasma wavelength obtained from SE analysis as a function of the resistivity for different In_2O_3 : TM samples, Previous experimental reported plasma energy of several TCOs are also shown [21,22] (b) The high-frequency dielectric constant of thin films vs N_{Hall} obtained from the intercept of the plot of ε_1 vs $1/(E^2 + \Gamma^2)$.

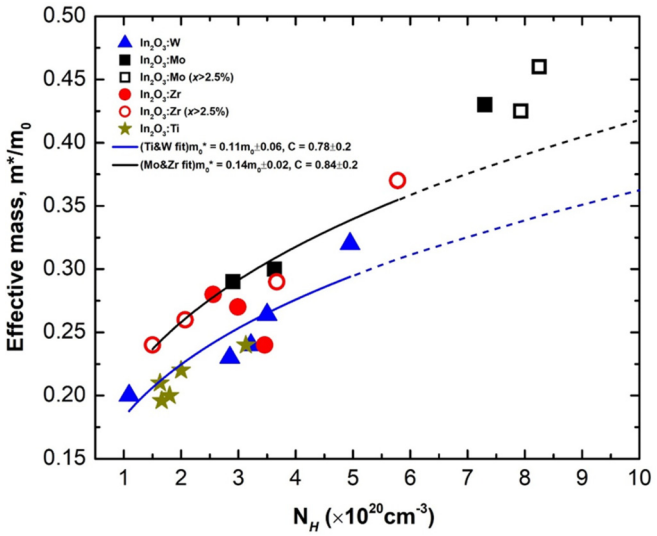

FIG. 6. Electron effective mass, m^* for In_2O_3 thin films with different dopants as a function of N_H, accuracies are $\sim \pm 5\%$, where m_o is the free electron mass. The black solid line is the best fit for the data from Mo and Zr doped while the black dashed line is the best fit for Ti- and W doped In_2O_3 samples of the conduction band nonparabolicity equation. The best fit curves were obtained for samples with $N_H < 5 \times 10^{20}$ cm^{-3}.

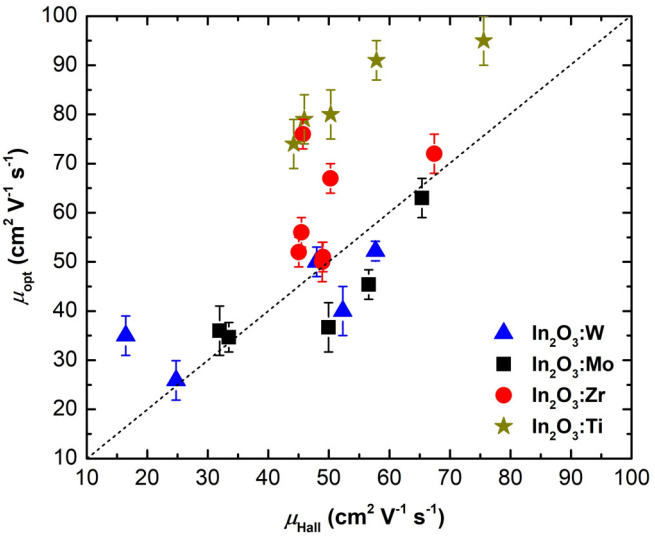

FIG. 7. Optical mobility of TM doped In_2O_3 obtained from the SE analysis as a function of Hall mobility.

agreement but slightly lower than previously reported values (e.g., Fujiwara *et al.*, reported ε_∞ value of ~3.98 for ITO film with $N_{\text{Hall}} \sim 1.2 \times 10^{21}$ cm^{-3} [22]).

C. Electron effective mass and optical mobility

To understand the origin of the higher mobility in the In_2O_3 : TM films, we extract their electron effective mass m^* using the expression for the plasma energy shown in Eq. (2), by assuming a time independent electric field. Hence, with the optical carrier density, $N_{\text{opt}} \approx N_H$ and using the values of ε_∞ in Fig. 5(b), the electron effective mass is obtained and the results are plotted as a function of N_H in Fig. 6. In the figure, the m^* for highly doped samples with $N_d > 2.5\%$ for Mo and Zr doped samples are plotted with open symbols. Figure 6 shows that the m^* increases with N_H, in particular, a more rapid increase is observed for In_2O_3:Mo at $N_H > 7 \times 10^{20}$ cm^{-3}. The increase in the m^* with N_H is consistent with the observed decrease in the Hall mobilities at high carrier concentration. We invoke the nonparabolicity of the conduction band to explain the dependence of the effective mass, m^* on N_H for In_2O_3 : TM thin films. The nonparabolicity of the conduction band can be expressed in terms of the nonparabolicity factor, C, using the analytical expression by Pisarkiewicz *et al.* [51] given as

$$m^* = m_0^* \sqrt{1 + 2C \frac{\hbar^2}{m_0^*} (3\pi^2 N)^{2/3}}, \tag{6}$$

where m_o^* is the effective mass at the conduction band minimum and N is the electron concentration which is taken as N_H. We also notice that the m^* for the Mo and Zr doped samples follows a slightly different curve from that for W and Ti doped ones. With m_o^* and C as the fitting parameters, the best fits for the effective mass data for Mo and Zr doped and W and Ti doped films with $N_H < 5 \times 10^{20}$ cm^{-3} are shown by the black and blue solid line respectively in Fig. 6. The best fit results for m_0^* and C are $\sim 0.14 \pm 0.02 m_o$ and 0.84 ± 0.2 eV^{-1}, respectively, where m_o is the free electron mass for the W and Ti doped samples. A slightly lower CB edge effective mass of $\sim 0.11 \pm 0.02 m_0$ with a C value of $\sim 0.78 \pm 0.1$ eV^{-1} is obtained for fitting using the data from the W and Ti doped samples. The obtained CB edge effective mass, m_o^* for In_2O_3 : TM from the fittings lie is the range of 0.11–0.14m_o, which is lower than previously reported values of m_o^* for In_2O_3 and In_2O_3 : Sn in the range of ~0.18–0.3m_o [22,52–54]. The smaller electron effective mass, m_o^* obtained here for samples with low carrier density $\sim N_H < 5 \times 10^{20}$ cm^{-3} supports the resonant doping picture described by Swallow *et al.* [8]. Table I also compares the electron effective mass of our In_2O_3 : TM samples to previously reported values. Figure 6 also shows that for $N_H > 5 \times 10^{20}$ cm^{-3}, the m^* deviates from the fits and is much higher than the fits (extrapolated in the dashed blue and black line). This much higher m^* at higher N_H (and also higher N_d) maybe related to the modification of the In_2O_3 conduction band by the anticrossing interaction of increased number of localized d states of the TM dopants with host conduction band states as described in Refs. [44,55,56].

The Drude broadening parameter Γ_D from the SE analysis [Eq. (1)] is also related to the optical mobility μ_{opt} and effective mass m^* from the expression $\Gamma_D = \frac{\hbar e}{m^* \mu_{\text{opt}}}$. The μ_{opt} determined from Γ_D and m^* for the In_2O_3 : TM thin films is plotted with respect to the Hall mobility, μ_{Hall} in Fig. 7. The dotted line in Fig. 7 indicates the case where $\mu_{\text{opt}} = \mu_{\text{Hall}}$. A reasonable correspondence of μ_{opt} with μ_{Hall} is shown for films doped with most TM species (W, Mo, and Zr), especially for films with $\mu_{\text{Hall}} < 50$ cm^2 V^{-1} s^{-1}. For the Ti doped sample with $\mu_{\text{Hall}} > 50$ cm^2 V^{-1} s^{-1}, large deviations with $\mu_{\text{opt}} > \mu_{\text{Hall}}$ are observed. Note that the optical mobility obtained from SE results describes the average mobility within the grain and is not affected by grain boundary scattering in polycrystalline

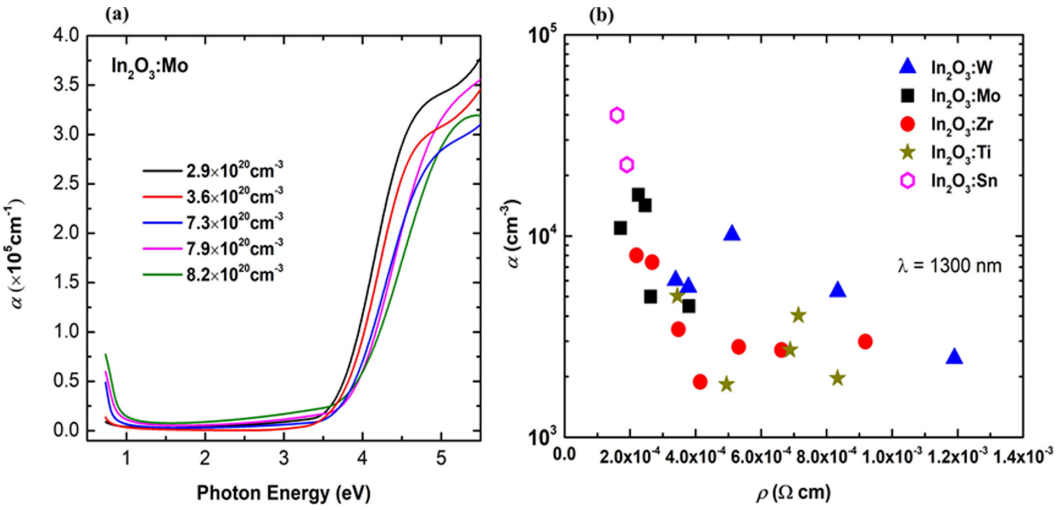

FIG. 8. (a) Absorption coefficient of Mo doped In_2O_3 for samples different N_{Hall}. (b) Free carrier absorption for values of TM doped In_2O_3 thin films at an IR wavelength of 1300 nm.

films, and hence is normally higher than the measured μ_{Hall}. In the case of Ti doping, high μ_{Hall} is obtained for samples with $N_d < 2\%$. At this low Ti doping, $N_H < 3 \times 10^{20}$ cm^{-3} and the effective mass $m^* < 0.25$ the ionized impurity scatterings are low. Hence grain boundary scatterings become more significant in reducing the μ_{Hall} as is observed in the plot of hall mobility vs hall electron concentration in Fig. S3 of Ref. [26]. Results shown in Fig. 7 also suggests that the mobility of Ti doped In_2O_3 can be further enhanced for films with larger grains by optimizing the growth as well as post-growth annealing conditions.

D. Free carrier absorption, transmission intensity, and optical band gap

Because of the high electron concentration in the In_2O_3 : TM, the free carrier absorption (FCA) becomes significant in the low photon energy region, $E < 1$ eV, and FCA increases with increasing N_H as shown in the absorption coefficient plots in Fig. 8(a) for In_2O_3:Mo thin films. The absorption coefficient spectra of the samples shown are obtained from SE spectra modelling. Due to the spectral range in the ellipsometry system used, we are limited to probing only up to 1700 nm and cannot show FCA data from samples with $N_H < 10^{20}$ cm^{-3}. The dependence of the absorption coefficient α with resistivity at the wavelength of 1300 nm in the NIR region is show in Fig. 8(b). For films with low $\rho \sim 1$–3×10^{-4} Ω cm, α for ITO films is much higher ($>2 \times 10^4$ cm^{-1}) due to FCA. In contrast, α for In_2O_3 : TM films are much lower ($< 10^4$ cm^{-1}), suggesting that In_2O_3 : TM films are better suited as transparent conductors on devices where transmission of longer wavelength photons is needed.

Figure 9(a) shows the transmission intensity of 150-nm-thick In_2O_3 thin films doped with different TM species for samples with resistivity in the range of $\rho \sim 1.07 \times 10^{-4}$-$3.4 \times 10^{-4}$ Ω cm. Transmission spectra of ITO films are shown

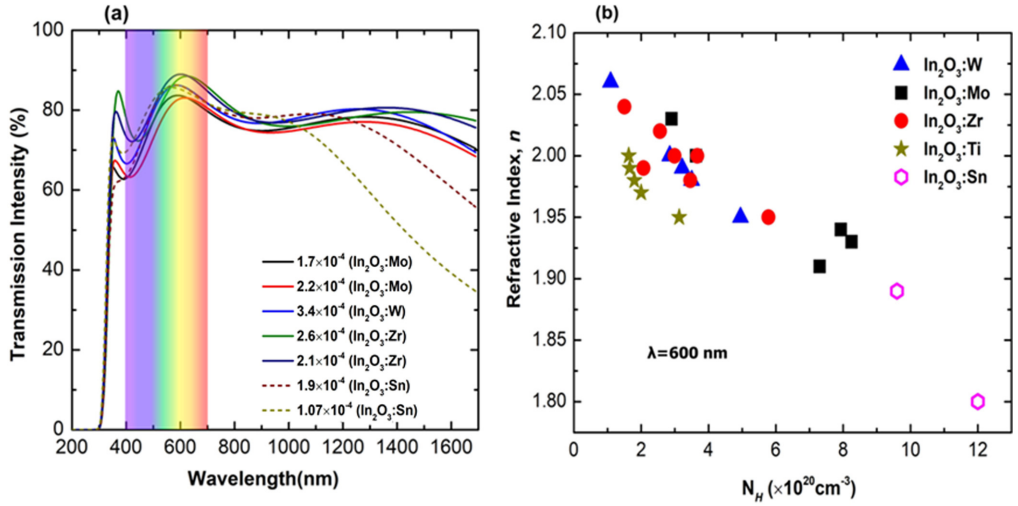

FIG. 9. (a) Optical transmission intensity of TM doped In_2O_3 thin films with thickness, $t = 150$ nm for different resistivity (Ω-cm), In_2O_3 : Sn thin films obtained at similar condition are also shown. (b) Refractive index n at 600 nm wavelength of the In_2O_3 thin films doped with various dopants obtained from SE Analysis.

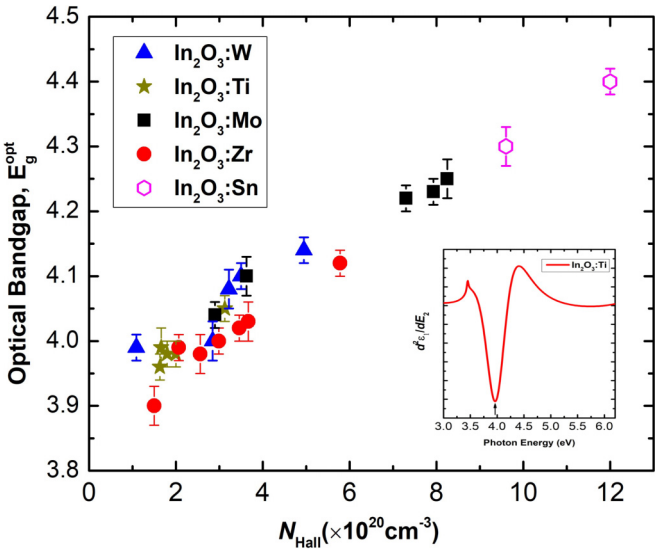

FIG. 10. Optical band gap of TM doped In_2O_3 thin films vs N_{Hall} obtained from the second derivative the real part of the dielectric function, $d^2\varepsilon_1/dE^2$. The inset shows $d^2\varepsilon_1/dE^2$ of a In_2O_3:Ti sample as a function of photon energy with the black arrow indicating the optical band-gap energy value.

as dashed lines for comparison. The ITO films with $\rho \sim 1.07$–$1.9 \times 10^{-4}\,\Omega$ cm show clear decrease in long wavelength transmittance with a remarkable decrease in transmittance at $\lambda > 1000$ nm for the ITO film with $\rho \sim 1.07 \times 10^{-4}\,\Omega$ cm due to the strong FCA [Fig. 8(b)] and the low λ_p [$\sim$1.2 μm from Fig. 5(a)]. However, TM doped thin films with ρ as low as $\sim 1.7 \times 10^{-4}\,\Omega$ cm show negligible decrease in NIR transmittance. From Fig. 9(a), In_2O_3:Mo thin films with $\rho \sim 1.7 \times 10^{-4}\,\Omega$ cm (black line) show transmittance$\sim$80% up to 1700 nm. This is a remarkable improvement in the transmittance compared to ITO films with similar conductivity due to the higher mobility in In_2O_3 : TM thin films.

To achieve the minimum light reflection and optimum transmittance in optoelectronic devices utilizing TCO, the refractive index of the TCO layer plays an important role. The refractive index of these In_2O_3 : TM thin films at the visible wavelength of 600nm is shown in Fig. 9(b). A monotonous decrease in the refractive index with increasing N_H of the films at the 600 nm is observed. In comparison, since ITO requires a higher N_H to achieve a comparably low resistivity as In_2O_3 : TM, and thus values of the refractive index for ITO samples are much lower ($n \sim 1.8$–1.9 compared to $\sim$1.9–2.0 for In_2O_3 : TM). The higher refractive index for In_2O_3 : TM is also a favorable attribute for optical coating applications [53].

Figure 10 shows the optical band gap E_g^{opt} of In_2O_3 : TM thin films as a function of N_H obtained from the second derivative of the real part of the dielectric function from SE analysis, $d^2\varepsilon_1/dE^2$. The optical band gap of ITO is also shown for comparison. An example of using the $d^2\varepsilon_1/dE^2$ method to obtain the of the optical band-gap energy for a In_2O_3:Ti sample is shown as the inset of Fig. 10 [57,58]. We found that using this method for determining the optical band gap for a degenerate semiconductor is more accurate than the conventional Tauc plot method and results in values similar to the method proposed by Dolgonos *et al.* [59]. In general, the Tauc plot underestimates the optical band gap in these thin films. Figure S4 [26] shows a comparison of the optical band gap of In_2O_3 : TM thin films obtained from Tauc method and the $d^2\varepsilon_1/dE^2$ method. Figure 10 shows a trend of increasing E_g^{opt} with N_H for different dopants. This increasing E_g^{opt} with N_H is attributed to the Burstein-Moss shift and band-gap renormalization effects observed for degenerately doped semiconductors [60,61].

V. CONCLUSION

Obtaining an ideal TCO with a high electrical conductivity and at the same time high transmittance over a wide spectral window (from UV to IR) posts a formidable challenge. This is because the high electron concentration required to achieve a high electrical conductivity in a TCO will also necessarily increase free carrier absorption and moves the plasma reflection wavelength to lower photon wavelength, and hence make the TCO not transparent in the NIR region. Transition metal doping in In_2O_3 provides an alternative to mitigate this trade off since the mobility in In_2O_3 : TM is improved and consequently a lower electron concentration is required to achieve a high conductivity comparable to the commonly used ITO. In this study, we explore the effects of free carriers on the transport and optical properties of TM (W, Zr, Mo, Ti) doped In_2O_3 thin films grown at low temperature by magnetron sputtering followed by RTA processing. The sputtered thin films showed higher mobilities for all TM dopants compared to ITO. In particular, a mobility of 75 cm^2/V-s is obtained for In_2O_3:Ti thin films with a carrier concentration of $\sim 2 \times 10^{20}$ cm^{-3}. Variable temperature measurements show a decrease in mobility with increasing temperature for high mobility In_2O_3 : TM due to phonon scattering. Detailed optical properties of In_2O_3 : TM films were studied by room temperature standard spectroscopic ellipsometry. Analyses of the SE data using dielectric function parameterization combining a Drude oscillator and several Tauc-Lorentz oscillators reveal the effects of free carriers on the complex dielectric function. Optical band gap shifts due to the Burstein-Moss and band-gap renormalization effects are also evident in these highly doped In_2O_3 thin films. Several material parameters useful for describing the electronic and optical properties of these In_2O_3 : TM films such as the plasma wavelengths λ_p, electron effective mass m*, high-frequency dielectric constant ε_∞, refractive index n, extinction coefficients k, and optical mobility μ_{opt} were obtained from our SE analysis. In general, a decrease of the ε_∞ and an increase in the plasma energy are observed with increasing carrier concentration. From the fittings of the electron effective mass using the nonparabolic conduction band model, the electron effective mass at the bottom of the conduction band m_o^* for In_2O_3 : TM are lower than that in ITO. Specifically, $m_o^* \sim 0.11$–$0.14 m_o$ is found for In_2O_3 : TM compared to the reported $m_o^* \sim 0.18$–$0.3 m_o$ for ITO. This is consistent with recent theoretical studies which proposed that $4d$ donor states of the TMs are resonance in the CB and do not disturb the CB dispersion of the host. For samples with high TM doping $N_d > 2.5\%$, the effective mass of In_2O_3 : TM films increases more rapidly and deviates

significantly from the CB nonparabolic model, resulting in a drastic drop in the mobility. This is in agreement with previous studies on TM doped ZnO and CdO which showed that at high dopant concentration anticrossing interactions of the TM *d* states with extended CB states results in the restructuring of the CB and significantly flattens the CB. Our study provides a detailed understanding of the optical properties in high mobility transparent TM doped In_2O_3 films. Using TM doping, we have achieved TCOs with conductivity comparable to ITO but with transmission extended to >1600 nm into the NIR spectral region. These materials will be potentially important as transparent conductors for optoelectronic devices utilizing the NIR photons.

The data that supports the findings of this study are available within the paper and Ref. [26].

ACKNOWLEDGMENTS

This work was supported by the General Research Fund of the Research Grants Council of Hong Kong SAR, China, under Project Nos. CityU 11305119 and CityU 11212118. C.P.L acknowledges the support of the start-up fund from Shantou University under Project No. NTF18027, Guangdong Basic and Applied Basic Research Foundation (Project No. 2020A 1515010180), Department of Science and Technology of Guangdong Province under Project No. 2021A0505030081, the Major Research Plan of the National Natural Science Foundation of China (Project No. 91950101), and the Optics and Photoelectronics Project (No. 2018KCXTDO11). K.O.E was supported by the Hong Kong Ph.D. Fellowship (PF16-02083) Research Grants Council, University Grants Committee, Hong Kong.

[1] X. Yu, T. J. Marks, and A. Facchetti, Metal oxides for optoelectronic applications, Nat. Mater. **15**, 383 (2016).

[2] M. Morales-Masis, S. De Wolf, R. Woods-Robinson, J. W. Ager, and C. Ballif, Transparent electrodes for efficient optoelectronics, Adv. Electron. Mater. **3**, 1600529 (2017).

[3] O. Bierwagen, Indium oxide - A transparent, wide-band gap semiconductor for (Opto)electronic applications, Semicond. Sci. Technol. **30**, 024001 (2015).

[4] A. Stadler, Transparent conducting oxides—an up-to-date overview, Materials (Basel) **5**, 661 (2012).

[5] Y. Shigesato, R. Koshi-ishi, T. Kawashima, and J. Ohsako, Early Stages of ITO Deposition on Glass or Polymer Substrates, Vacuum **59**, 614 (2000).

[6] Y. Park, V. Choong, Y. Gao, B. R. Hsieh, and C. W. Tang, Work function of indium tin oxide transparent conductor measured by photoelectron spectroscopy, Appl. Phys. Lett. **68**, 2699 (1996).

[7] H. Peelaers, E. Kioupakis, and C. G. Van de Walle, Limitations of In_2O_3 as a transparent conducting oxide, Appl. Phys. Lett. **115**, 082105 (2019).

[8] J. E. N. Swallow, B. A. D. Williamson, S. Sathasivam, M. Birkett, T. J. Featherstone, P. A. E. Murgatroyd, H. J. Edwards, Z. W. Lebens-Higgins, D. A. Duncan, M. Farnworth, P. Warren, N. Peng, T. L. Lee, L. F. J. Piper, A. Regoutz, C. J. Carmalt, I. P. Parkin, V. R. Dhanak, D. O. Scanlon, and T. D. Veal, Resonant doping for high mobility transparent conductors: the case of Mo doped In_2O_3, Mater. Horizons **7**, 236 (2020).

[9] S. Parthiban, K. Ramamurthi, E. Elangovan, R. Martins, and E. Fortunato, Spray deposited molybdenum doped indium oxide thin films with high near infrared transparency and carrier mobility, Appl. Phys. Lett. **94**, 212101 (2009).

[10] E. Aydin, M. De Bastiani, X. Yang, M. Sajjad, F. Aljamaan, Y. Smirnov, M. N. Hedhili, W. Liu, T. G. Allen, L. Xu, E. Van Kerschaver, M. Morales-Masis, U. Schwingenschlögl, and S. De Wolf, Zr doped indium oxide (IZRO) transparent electrodes for perovskite-based tandem solar cells, Adv. Funct. Mater. **29**, 1901741 (2019).

[11] T. Koida, and M. Kondo, Improved near-infrared transparency in sputtered In_2O_3-based transparent conductive oxide thin films by Zr-doping, J. Appl. Phys. **101**, 063705 (2007).

[12] S. Kumar Vishwanath, T. An, W. Y. Jin, J. W. Kang, and J. Kim, The optoelectronic properties of tungsten doped indium oxide thin films prepared by polymer-assisted solution processing for use in organic solar cells, J. Mater. Chem. C **5**, 10295 (2017).

[13] R. Hashimoto, Y. Abe, and T. Nakada, High mobility titanium doped In_2O_3 thin films prepared by sputtering/post-annealing technique, Appl. Phys. Express **1**, 015002 (2008).

[14] F. Meng, J. Shi, Z. Liu, Y. Cui, Z. Lu, and Z. Feng, High mobility transparent conductive W doped In_2O_3 thin films prepared at low substrate temperature and its application to solar cells, Sol. Energy Mater. Sol. Cells **122**, 70 (2014).

[15] T. Koida and M. Kondo, High-mobility transparent conductive Zr doped In_2O_3, Appl. Phys. Lett. **89**, 082104 (2006).

[16] S. Parthiban, V. Gokulakrishnan, K. Ramamurthi, E. Elangovan, R. Martins, E. Fortunato, and R. Ganesan, High near-infrared transparent molybdenum doped indium oxide thin films for nanocrystalline silicon solar cell applications, Sol. Energy Mater. Sol. Cells **93**, 92 (2009).

[17] D. S. Bhachu, D. O. Scanlon, G. Sankar, T. D. Veal, R. G. Egdell, G. Cibin, A. J. Dent, C. E. Knapp, C. J. Carmalt, and I. P. Parkin, Origin of high mobility in molybdenum doped indium oxide, Chem. Mater. **27**, 2788 (2015).

[18] H. Li, S. Yin, G. Dong, G. Cui, C. Lei, Y. Li, X. Xu, L. Feng, J. Zhang, and C. Yu, Effect of humidity on optical and electrical properties of Zr doped In_2O_3 and a new structure for transparent electrode of silicon heterojunction solar cell, Sol. Energy **196**, 125 (2020).

[19] M. Morales-Masis, E. Rucavado, R. Monnard, L. Barraud, J. Holovsky, M. Despeisse, M. Boccard, and C. Ballif, Highly conductive and broadband transparent Zr doped In_2O_3 as front electrode for solar cells, IEEE J. Photovoltaics **8**, 1202 (2018).

[20] E. Rucavado, F. Landucci, M. Döbeli, Q. Jeangros, M. Boccard, A. Hessler-Wyser, C. Ballif, and M. Morales-Masis, Zr doped indium oxide electrodes: annealing and thickness effects on microstructure and carrier transport, Phys. Rev. Mater. **3**, 084608 (2019).

[21] C. P. Liu, Y. Foo, M. Kamruzzaman, C. Y. Ho, J. A. Zapien, W. Zhu, Y. J. Li, W. Walukiewicz, and K. M. Yu, Effects of Free Carriers on the Optical Properties of Doped CdO for Full-Spectrum Photovoltaics, Phys. Rev. Appl. **6**, 064018 (2016).

[22] H. Fujiwara and M. Kondo, Effects of carrier concentration on the dielectric function of ZnO:Ga and In_2O_3:Sn studied by spectroscopic ellipsometry: analysis of free-carrier and band-edge absorption, Phys. Rev. B **71**, 075109 (2005).

[23] K. O. Egbo, C. P. Liu, C. E. Ekuma, and K. M. Yu, Vacancy defects induced changes in the electronic and optical properties of nio studied by spectroscopic ellipsometry and first-principles calculations, J. Appl. Phys. **128**, 135705 (2020).

[24] K. O. Egbo, C. E. Ekuma, C. P. Liu, and K. M. Yu, Efficient p -type doping of sputter-deposited NiO thin films with Li, Ag, and Cu acceptors, Phys. Rev. Mater. **4**, 104603 (2020).

[25] M. Ohring, *The Material Science of Thin Films* (Academic Press, San Diego, California, 1991).

[26] See Supplemental Material at http://link.aps.org/supplemental/10.1103/PhysRevMaterials.5.094603 for the XRD spectra, data showing the changes in the electrical properties of In_2O_3 : TM thin films with annealing temperature, details of the dielectric function oscillator parameters used in SE Modelling, the plot of hall density versus hall mobility and the comparison of optical band gap extracted from different methods.

[27] Fox Mark, *Optical Properties of Solids*, 2nd ed. (Oxford University Press, Oxford, UK, 2010).

[28] J. Hilfiker and T. Tiwald, Dielectric function modeling, in *Spectroscopic Ellipsometry for Photovoltaics Volume 1: Fundamental Principles and Solar Cell Characterization*, edited by H. Fujiwara and R. Collins (Springer International, Switzerland, AG, 2018), pp. 115–153.

[29] I. Chatratin, F. P. Sabino, P. Reunchan, S. Limpijumnong, J. B. Varley, C. G. Van de Walle, and A. Janotti, Role of point defects in the electrical and optical properties of In_2O_3, Phys. Rev. Mater. **3**, 074604 (2019).

[30] F. Oba, M. Choi, A. Togo, A. Seko, and I. Tanaka, Native defects in oxide semiconductors: a density functional approach, J. Phys. Condens. Matter **22**, 384211 (2010).

[31] A. Lyubchyk, A. Vicente, B. Soule, P. U. Alves, T. Mateus, M. J. Mendes, H. Águas, E. Fortunato, and R. Martins, Mapping the electrical properties of ZnO-based transparent conductive oxides grown at room temperature and improved by controlled postdeposition annealing, Adv. Electron. Mater. **2**, 1500287 (2016).

[32] J. Jia, S. Iwasaki, S. Yamamoto, S. Nakamura, E. Magome, T. Okajima, and Y. Shigesato, Temporal evolution of microscopic structure and functionality during crystallization of amorphous indium-based oxide films, ACS Appl. Mater. Interfaces **13**, 31825 (2021).

[33] J. Xu, J. B. Liu, B. X. Liu, S. N. Li, S. H. Wei, and B. Huang, Design of n-type transparent conducting oxides: the case of transition metal doping in In_2O_3, Adv. Electron. Mater. **4**, 1700553 (2018).

[34] Y. Meng, X. Yang, H. Chen, J. Shen, Y. Jiang, Z. Zhang, and Z. Hua, Molybdenum doped indium oxide transparent conductive thin films, J. Vac. Sci. Technol. A Vacuum, Surfaces, Film. **20**, 288 (2002).

[35] N. Yamada, M. Yamada, H. Toyama, R. Ino, X. Cao, Y. Yamaguchi, and Y. Ninomiya, High-throughput optimization of near-infrared-transparent Mo doped In_2O_3 thin films with high conductivity by combined use of atmospheric-pressure mist chemical-vapor deposition and sputtering, Thin Solid Films **626**, 46 (2017).

[36] Y. Yoshida, D. M. Wood, T. A. Gessert, and T. J. Coutts, High-mobility, sputtered films of indium oxide doped with molybdenum, Appl. Phys. Lett. **84**, 2097 (2004).

[37] S. Parthiban, E. Elangovan, K. Ramamurthi, R. Martins, and E. Fortunato, Investigations on high visible to near infrared transparent and high mobility Mo doped In_2O_3 thin films prepared by spray pyrolysis technique, Sol. Energy Mater. Sol. Cells **94**, 406 (2010).

[38] X. Li, W. Miao, Q. Zhang, L. Huang, Z. Zhang, and Z. Hua, The electrical and optical properties of molybdenum doped indium oxide films grown at room temperature from metallic target, Semicond. Sci. Technol. **20**, 823 (2005).

[39] M. V. Frischbier, H. F. Wardenga, M. Weidner, O. Bierwagen, J. Jia, Y. Shigesato, and A. Klein, Influence of dopant species and concentration on grain boundary scattering in degenerately doped In_2O_3 thin films, Thin Solid Films **614**, 62 (2016).

[40] M. F. A. M. Van Hest, M. S. Dabney, J. D. Perkins, D. S. Ginley, and M. P. Taylor, Titanium doped indium oxide: a high-mobility transparent conductor, Appl. Phys. Lett. **87**, 032111 (2005).

[41] M. Yang, J. Feng, G. Li, and Q. Zhang, Tungsten doped In_2O_3 transparent conductive films with high transmittance in near-infrared region, J. Cryst. Growth **310**, 3474 (2008).

[42] Y. Liu, S. Zhu, R. Wei, L. Hu, X. Tang, J. Yang, W. Song, J. Dai, X. Zhu, and Y. Sun, Solution processed W doped In_2O_3 thin films with high carrier mobility, Ceram. Int. **46**, 2173 (2020).

[43] P. F. Newhouse, C. H. Park, D. A. Keszler, J. Tate, and P. S. Nyholm, High electron mobility w doped In_2O_3 thin films by pulsed laser deposition, Appl. Phys. Lett. **87**, 112108 (2005).

[44] Y. J. Li, K. M. Yu, G. B. Chen, C. P. Liu, and W. Walukiewicz, Conduction band modifications by d states in vanadium doped CdO, J. Alloys Compd. **822**, 153567 (2020).

[45] E. García-Hemme, K. M. Yu, P. Wahnon, G. González-Díaz, and W. Walukiewicz, Effects of the d-donor level of vanadium on the properties of $Zn_{1-x}V_xO$ films, Appl. Phys. Lett. **106**, 182101 (2015).

[46] M. Xie, W. Zhu, K. M. Yu, Z. Zhu, and G. Wang, Effects of doping and rapid thermal processing in Y doped CdO thin films, J. Alloys Compd. **776**, 259 (2019).

[47] Y. Yang, S. Jin, J. E. Medvedeva, J. R. Ireland, A. W. Metz, J. Ni, M. C. Hersam, A. J. Freeman, and T. J. Marks, CdO as the archetypical transparent conducting oxide. systematics of dopant ionic radius and electronic structure effects on charge transport and band structure, J. Am. Chem. Soc. **127**, 8796 (2005).

[48] N. Preissler, O. Bierwagen, A. T. Ramu, and J. S. Speck, Electrical transport, electrothermal transport, and effective electron mass in single-crystalline In_2O_3 films, Phys. Rev. B **88**, 085305 (2013).

[49] J. Jia, N. Oka, M. Kusayanagi, S. Nakatomi, and Y. Shigesato, Origin of carrier scattering in polycrystalline Al-doped ZnO films, Appl. Phys. Express **7**, 105802 (2014).

[50] E. Kaxiras, and J. Joannopoulos, *Quantum Theory of Materials*, 1st ed. (Cambridge University Press, Cambridge, UK, 2019).

[51] T. Pisarkiewicz, K. Zakrzewska, and E. Leja, Scattering of charge carriers in transparent and conducting thin oxide films with a non-parabolic conduction band, Thin Solid Films **174**, 217 (1989).

[52] M. Feneberg, J. Nixdorf, C. Lidig, R. Goldhahn, Z. Galazka, O. Bierwagen, and J. S. Speck, Many-electron effects on the

dielectric function of cubic In_2O_3: effective electron mass, band nonparabolicity, band gap renormalization, and burstein-moss shift, Phys. Rev. B **93**, 045203 (2016).

[53] M. Stokey, R. Korlacki, S. Knight, A. Ruder, M. Hilfiker, Z. Galazka, K. Irmscher, Y. Zhang, H. Zhao, V. Darakchieva, and M. Schubert, Optical phonon modes, static and high-frequency dielectric constants, and effective electron mass parameter in cubic In_2O_3, J. Appl. Phys **129**, 225102 (2021).

[54] K. H. L. Zhang, R. G. Egdell, F. Offi, S. Iacobucci, L. Petaccia, S. Gorovikov, and P. D. C. King, microscopic Origin of Electron Accumulation in In_2O_3, Phys. Rev. Lett. **110** 056803 (2013).

[55] W. Shan, W. Walukiewicz, J. W. Ager, E. E. Haller, J. F. Geisz, D. J. Friedman, J. M. Olson, and S. R. Kurtz, Band Anticrossing in GaInNAs Alloys, Phys. Rev. Lett. **82**, 1221 (1999).

[56] W. Walukiewicz, W. Shan, K. M. Yu, J. W. Ager, E. E. Haller, I. Miotkowski, M. J. Seong, H. Alawadhi, and A. K. Ramdas, Interaction of Localized Electronic States with the Conduction Band: Band Anticrossing in II-VI Semiconductor Ternaries, Phys. Rev. Lett. **85**, 1552 (2000).

[57] C. P. Liu, K. O. Egbo, C. Y. Ho, Y. Wang, C. K. Xu, and K. M. Yu, Wide-Gap $Zn_{1-x}Ni_xO$ Alloy: A Transparent p -Type Oxide, Phys. Rev. Appl. **13**, 024049 (2020).

[58] K. O. Egbo, M. Kong, C. P. Liu, and K. M. Yu, Room temperature sputtered Cu Doped $NiO_{1+\delta}$: P-type conductivity, stability of electrical properties and p-n eterojunction, J. Alloys Compd. **835**, 155269 (2020).

[59] A. Dolgonos, T. O. Mason, and K. R. Poeppelmeier, Direct optical band gap measurement in polycrystalline semiconductors: a critical look at the tauc method, J. Solid State Chem. **240**, 43 (2016).

[60] E. Burstein, Anomalous optical absorption limit in InSb, Phys. Rev. **93**, 632 (1954).

[61] A. Walsh, J. L. F. Da Silva, and S. H. Wei, Origins of band-gap renormalization in degenerately doped semiconductors, Phys. Rev. B **78**, 075211 (2008).